The wake of an actuator line with a vortex-based tip/smearing correction in uniform and turbulent inflow

Meyer Forsting, Alexander R.; Pirrung, Georg R.; Ramos García, Néstor

Published in:
Proceedings of the Wake Conference 2019

Link to article, DOI:
10.1088/1742-6596/1256/1/012020

Publication date:
2019

Document Version
Publisher's PDF, also known as Version of record

The wake of an actuator line with a vortex-based tip/smearing correction in uniform and turbulent inflow

IOP Conf. Series: Journal of Physics: Conf. Series **1256** (2019) 012020 doi:10.1088/1742-6596/1256/1/012020

The wake of an actuator line with a vortex-based tip/smearing correction in uniform and turbulent inflow

Alexander R Meyer Forsting[1], Georg R. Pirrung[1], Néstor Ramos-García[1]

[1] DTU Wind Energy, Technical University of Denmark, Frederiksborgvej 399, 4000 Roskilde, Denmark

E-mail: alrf@dtu.dk

Abstract. The force smearing in the actuator line technique ensures its numerical stability, but also breaks its intended similarity to the lifting line by similarly smearing its vorticity in the flow domain. The wake thus induces lower velocities at the blade, linking the blade forces to the force smearing. A recently developed tuning-free, vortex-based correction recovers this missing induction, regaining the lifting-line behaviour of the actuator line. The interplay of this new smearing correction with grid and blade resolution is studied in uniform and turbulent inflow with respect to the blade forces and wake behaviour. With only 10 grid cells along the blade, the thrust is within 2.8% and the power within 5.7% of the high-resolution reference. With 20 grid cells the difference drops to 1.5% and 2.5%, respectively. The influence of the force smearing on the wake velocities dominates over the choice of correction, yet under turbulent inflow the wake characteristics become nearly independent of force smearing 6 rotor radii downstream of the turbine.

1. Introduction

The actuator line (AL) technique developed by Sørensen and Shen [1] is a lifting-line (LL) representation of the wind turbine rotor suitable for computational fluid dynamics (CFD) simulations. It captures transient physical features like shed and trailed vorticity (including root/tip vortices), without the computational cost associated with resolving the full rotor geometry.

Different to LL vortex formulations the blade forces are dispersed in the flow domain - most commonly in form of a Gaussian projection - to avoid numerical instability. A length scale - also referred to as smearing factor - controls this force redistribution, whose lower limit is linked to the grid size through numerical stability requirements [2]. Shives *et al.* documented the similarity between the velocities induced across an AL with Gaussian force smearing and those predicted by a viscous vortex core model [3]. Dag *et al.* [4] identified the Lamb-Oseen [5, 6] vortex as best match to empirical observations - this equivalence was later confirmed theoretically [7, 8]. Following their observations, Dag *et al.* postulated that the trailed vorticity inherits the viscous core from the bound vortex of the AL, inducing lower velocities at the blade than without the core and force smearing. This assumption was verified both empirically [7] and theoretically [8],

but only holds for three-dimensional Gaussian force smearing. Dag *et al.* proposed correcting the AL by estimating the missing velocity from LL simulations.

Based on this, we recently developed a smearing correction [7] - not tip correction as it does not correct for the physical deficiencies of BEM methods - that incorporates the viscous core in the dynamic near-wake model [9, 10]. Our implementation was validated with LL simulations of the NREL 5MW turbine at different wind speeds as shown in figure 1, where the correction leads to AL blade force distributions matching LL results (refer to section 3.2 for details on the LL method). The figure also shows that LL simulations with trailing vortices exhibiting viscous cores (LL + core) lead to similar forces as an AL without any correction.

In this paper we investigate the interplay of smearing/tip corrections and grid resolution with respect to the blade forces and wake of the NREL 5MW rotor. The new correction could potentially allow wind farm simulations at lower grid resolution than usual, without jeopardising their accuracy.

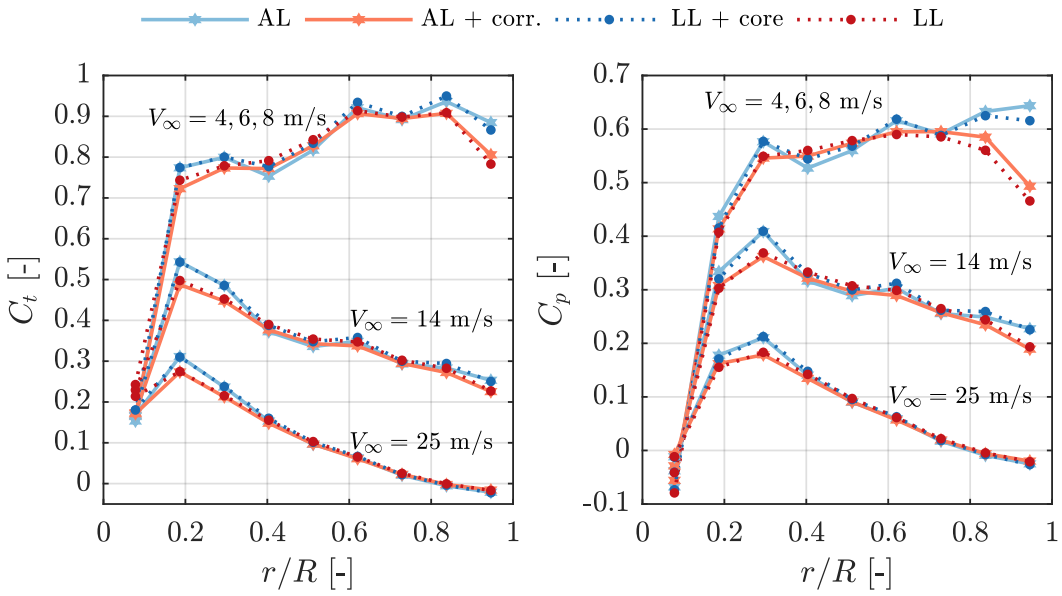

Figure 1. Local thrust and power coefficients along the NREL 5MW blades at different wind speeds predicted by AL simulations with/without smearing correction and LL with/without core. ($N_s = 9$, $\Delta x = R/10$, $\epsilon = 0.2R$)

2. Smearing correction for the actuator line

The correction relies on representing the rotor wake with trailed vortices. They are shed in-between the AL blade sections as shown in figure 2 with a strength of $\Delta\Gamma = \Gamma_s - \Gamma_{s+1}$ - the change in bound circulation from one section s to a neighbouring one. An infinitesimal element of this trailed vortex δl induces a velocity δu at an arbitrary point C along the blade. We estimate this increment with the near-wake model (NWM) of Pirrung *et al.* [9, 10]. This model assumes a fixed-wake to arrive at a simple fit to the analytical expressions for the induced velocities, which derive from the Biot-Savart law. It relies on indicial functions and thus time-advancement is achieved by a mere multiplication. However the NWM gives the velocity induced by an inviscid vortex - to arrive at the missing velocity introduced by the viscous core, the induced velocity

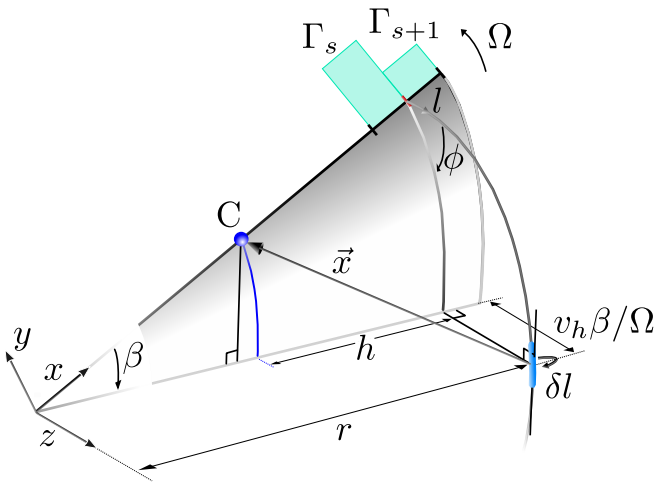

Figure 2. Trailed vorticity path. The blade rotates in the x-y plane and z points downstream. The vortex element δl with strength $\Gamma_s - \Gamma_{s+1}$ is shed at r and transported downstream by the local velocity. The distance from the shedding location r to a point C along the blade is h ($h = r - C_x$), where δl induces tangential and axial velocities.

needs to be multiplied by the smearing function

$$f_\epsilon = \exp\left(-\frac{(\mathbf{x}\hat{\mathbf{e}}_\perp)^2}{\epsilon^2}\right) \tag{1}$$

,with ϵ representing the smearing length scale. The viscous core only acts in the plane orthogonal to the vortex element $\delta\mathbf{l}$, hence the direction vector $\hat{\mathbf{e}}_\perp$ normal to it, projects the vector $\mathbf{x}$ pointing towards the point C from the element, onto this orthogonal plane.

The total missing induction at a blade section s is obtained by summing the contribution from all trailed vortices. The number of trailed vortices N_v is directly related to the number of sections resolving the aerodynamic characteristics of the blade, $N_v = N_s + 1$. Discretising the vortices in time, the missing induction at a certain blade section becomes

$$\mathbf{u}_s^\star = \sum_v^{N_v} \sum_n^{N_t} f_{s,v}^n \boldsymbol{\Delta}\tilde{\mathbf{u}}_{s,v}^n \tag{2}$$

Here v denotes the trailed vortex index, n the time index and N_t the number of time steps. As $f_{s,v}^n$ is a function of time - due to the term $\mathbf{x}\hat{\mathbf{e}}_\perp$ in equation (1) - the original NWM was modified to include this time dependency in [7].

Finally the missing velocities computed in equation (2) correct the original velocities from the CFD simulations

$$\mathbf{u}_s = \mathbf{u}_s^{\mathrm{CFD}} + \mathbf{u}_s^\star \tag{3}$$

The correction has a large impact towards the root and tip of the blade by reducing the angle-of-attack in this region. The influence on the velocity magnitude and the corresponding change in the blade forces is negligible.

For a more detailed presentation and discussion of the smearing correction see [7].

3. Computational method

3.1. Actuator-line simulations

The discretised incompressible Navier-Stokes equations are solved with DTU's CFD code EllipSys3D [11, 12, 13]. Details on the numerical techniques are given in [14]. With uniform inflow the RANS equations are solved using the k-ω shear-stress transport turbulence closure of Menter [15], whereas the turbulent inflow cases in section 4.2 are computed with the DES technique of Strelets [16]. The AL model was implemented by Mikkelsen *et al.* [17] in EllipSys3D. We employ a version utilising three-dimensional Gaussian force projection, which follows the original formulation by Sørensen and Shen [1]. The smearing length scale is at least twice the grid size as recommended by Troldborg *et al.*[2] to guarantee numerical stability and the time resolution ensures the blade tip to move no further than one grid cell during a step. A detailed description of the numerical domain for the uniform inflow cases is given in [7]. To investigate the wake evolution under turbulent conditions, the mesh was extended in the streamwise direction, such that the box domain encompassed $20R$ x 20R x $25R$, with R representing the rotor radius. The refined mesh extended from the inflow plane until $16R$ downstream, with the rotor located $6R$ from the inflow boundary. The mesh size for this set of simulations was set to $R/32$ independent of blade resolution. Thereby all changes in the wake originate purely from the blade definition and corresponding force smearing, not from the interaction of the turbulence with the mesh. The isotropic Mann turbulence boxes [18] are those detailed in [14].

3.2. Free-wake lifting-line rotor simulations

The in-house solver MIRAS has been employed to perform the free-wake lifting-line simulations. MIRAS is a multi-fidelity computational vortex model, which is mainly used for predicting the aerodynamic behaviour of wind turbines and its wakes [19, 20, 21].

The free-wake vortex method essentially models the wake of a wind turbine by a bundle of infinitely thin vortex filaments. For the sake of the present study, two different approaches to compute the angle of attack have been followed.

- Inviscid (LL), where the non-regularized Biot-Savart law is used to compute the induction from the wake filaments at the quarter-chord location. This is the standard method used in lifting line solvers.
- Viscous (LL+core), where the regularised Biot-Savart law is used to compute the induction at the quarter-chord location. A viscous core with radius equal to the actuator line smearing factor is used for a direct comparison of the methods.

This enables a double validation of the models. On one hand the corrected AL simulations can be validated against the LL calculations, and on the other hand the raw AL model, without tip correction, can be compared against the LL+core simulations which include the smearing effect in the free-wake model. It is important to note here that in all LL simulations a viscous core model is used during the filament position updating procedure in order to avoid the singular behaviour of the Biot-Savart law. In this case the initial core radius has been set to 0.1% of the local chord. A dynamic viscous core model is applied to emulate the effect of viscosity by changing the vortex core radius as a function of time as in [19].

4. Results and Discussion

All results are obtained with a stiff AL representation of the NREL 5MW [23] running at a mean wind speed of 8 $\mathrm{m\,s^{-1}}$ with 9.2 rpm and zero pitch - hub and nacelle are not included. Operating at its maximal thrust and power coefficient, tip corrections have their largest relative impact on the blade forces in this regime (see figure 1). Contrary to tip corrections, the smearing correction also significantly improves the blade loading towards the blade root at higher wind speeds, as demonstrated in [7].

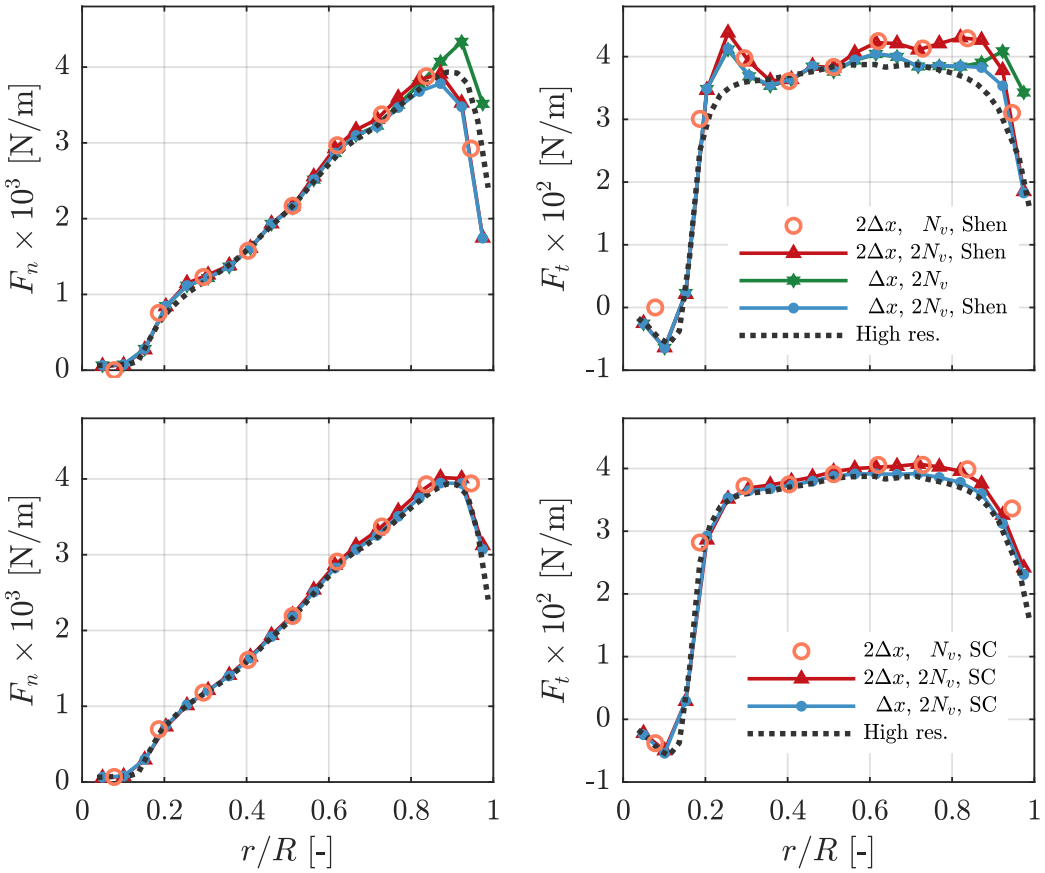

Figure 3. Normal and tangential forces on the NREL 5MW blades at 8 $\mathrm{m\,s^{-1}}$ predicted by AL simulations with different combinations of blade and grid resolution. The upper panel shows results with the tip correction of Shen *et al.* [22] and without correction, the lower one the same cases with the smearing correction (SC) [7]. ($N_v = 10$, $\Delta x = R/20$; $\epsilon = 2\Delta x$; High res.: $N_v = 40$ + SC)

4.1. Uniform inflow

4.1.1. Blade forces Figure 3 compares the effect of Shen's tip correction [22] - with the original coefficients- and the smearing correction (SC) on the blade forces of the NREL turbine and investigates their interplay with blade and grid resolution. Here the lowest grid resolution is $2\Delta x$ or $R/10$ and the blade is discretised by either 9 ($N_v - 1$) or 19 sections ($2N_v - 1$). As reference acts a high resolution (High res.) AL simulation with $\Delta x = R/40$, 40 blade sections and with active smearing correction to arrive at a LL equivalent solution. Clearly, the simulations with Shen's correction exhibit a stronger dependency on grid resolution. Doubling the blade resolution without a corresponding change in the grid definition does not yield an improved force distribution, but only increases the resolution of the exact same forces. Unsurprisingly, greater mesh resolution does not benefit the inboard loading, as the tip correction only acts in the outer fifth of the blade. Whereas the normal forces are excessively reduced towards the tip, the tangential forces are not sufficiently diminished. This originates from Shen's correction acting equally on both forces, which was identified by Wimshurst *et al* [24] to disagree with the actual tip loss mechanism observed for turbines (also see Pirrung *et al.*[25] for an adapted correction).

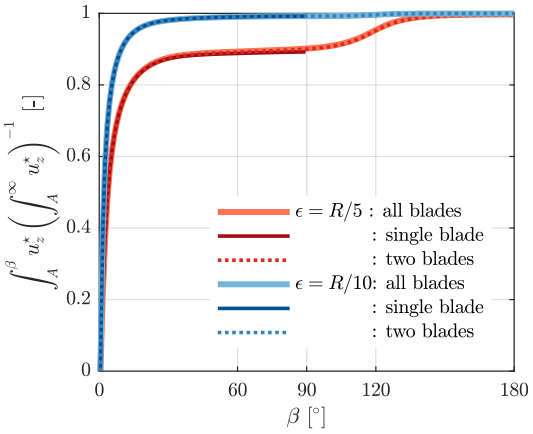

Figure 4. Normalised build-up rotor-averaged, normal induction correcting velocities with wake length as predicted by a fixed-wake approach.

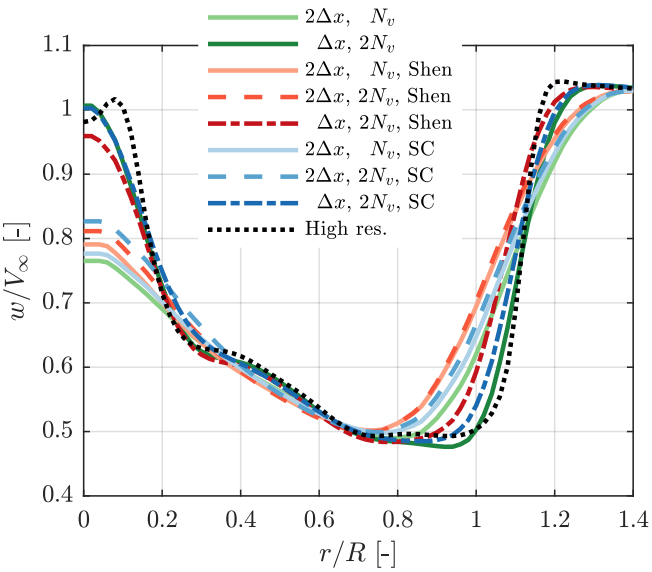

Figure 5. Azimuthally averaged wake deficit one rotor radius downstream of the NREL 5MW at 8 $\mathrm{m\,s^{-1}}$ uniform inflow predicted by AL simulations with different combinations of blade and grid resolution, with/without tip/smearing correction. ($N_v = 10$, $\Delta x = R/20$; High res.: $N_v = 40$ + SC)

Contrary, the smearing correction (SC) improves both load distributions, with a slight over-prediction of the forces towards the tip - maximally 3% in the normal and 6% in the tangential component at the lowest grid resolution, falling to 0.5% and 2%, respectively, when halving the mesh size. Thus a more accurate force distribution can be obtained even at low grid resolution, which reduces the computational costs of aero-elastically coupled simulations. The remaining dependency on the smearing parameter partially related to ignoring the velocities induced by other blades. Figure 4 shows the build up of the velocities correcting the normal induction with wake length for the two cases presented in figure 3. Here the focus is on the normal component of the velocity correction, as it has the greatest impact on the forces through the angle-of-attack. The velocities are obtained by numerically solving the Biot-Savart law for a fixed-wake, as defined in figure 2. In the current smearing correction, the trailed vorticity only affects the blade from which it is shed. Figure 4 shows that for large force smearing the induction from the remaining blades' vorticity (notice the increase at 120° and 240°) contributes 11% at $\epsilon = R/5$ and less then 1% at half the smearing length scale. Overall, the induction from other blades is probably not the main reason for the remaining dependency on the length scale and needs further investigation.

4.1.2. Wakes Little attention is usually given to the wake behaviour in connection with tip corrections, despite their mutual interaction through the blade forces. figure 5 compares the near-wake profiles - one radius from the rotor plane - for the blade load distributions presented in figure 3. Generally, the wake deficit exhibits little sensitivity to the correction, but instead is connected to the grid resolution through the smearing factor. At the lower resolution ($2\Delta x$) $\epsilon = R/5$, which leads to less pronounced shear layers at the outer edge of the wake and towards the root. This large force smearing, furthermore, significantly reduces the mass flow in the wake centre. The change in momentum flux is closest to the highly resolved solution for simulations

Table 1. Change in momentum flux for the cases in figure 5 one rotor radius downstream of the rotor plane with respect to the highly resolved (High res.) simulation.

Case	$R/\Delta x$	R/ϵ	N_v	$\Delta \int (w^2 - w_\infty^2) dA$ [%]
no corr.	10	5	10	−1.10
Shen			10	1.00
			20	1.29
SC			10	−0.30
			20	0.37
no corr.	20	10	20	−0.99
Shen				1.00
SC				0.22

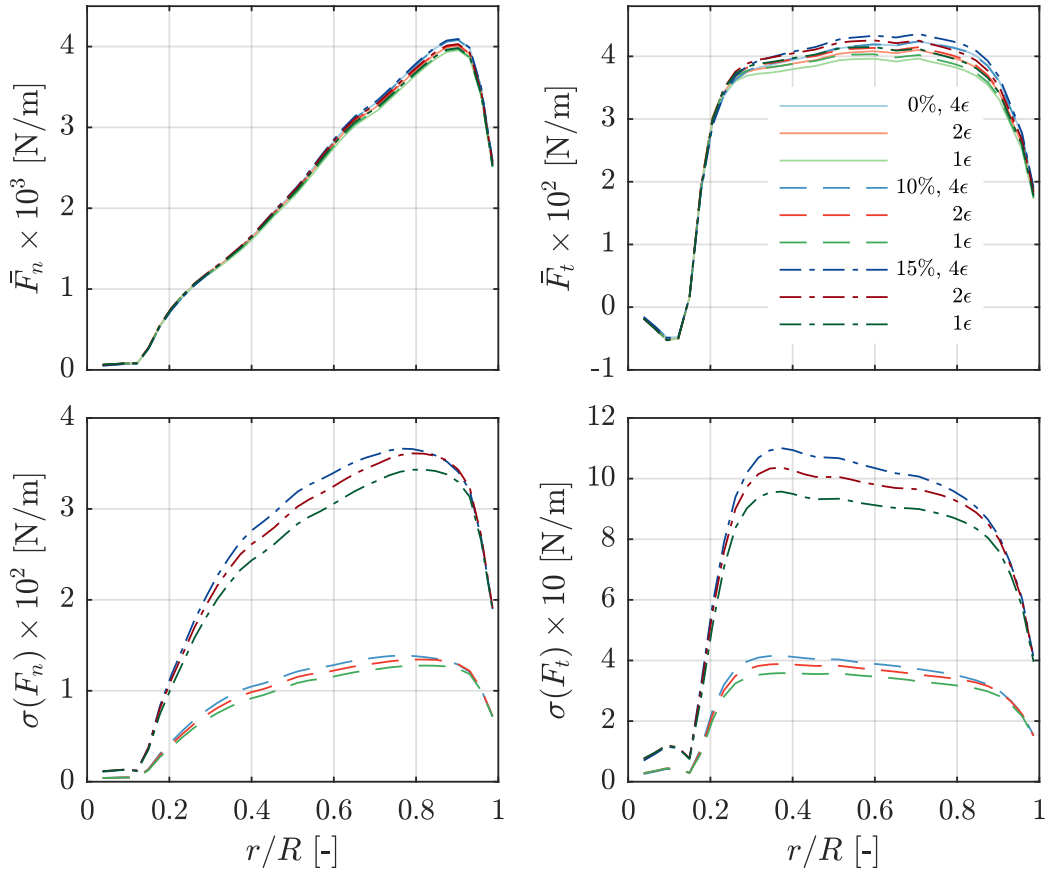

Figure 6. 10-minute average and standard deviation of normal and tangential forces on the NREL 5MW at 8 m s^{-1} mean wind speed and three inflow turbulence levels (0%, 5%, 10%) and with three different smearing length scales. ($N_v = 36$, $\Delta x = R/32$, $\epsilon = R/16$)

using the SC as presented in table 1. With a grid resolution of $\Delta x = R/20$ and active SC, the wake profile approaches the reference, whereas the outer wake edge moves inboard with Shen's tip correction.

4.2. Turbulent inflow

4.2.1. Blade forces As previously shown by Troldborg *et al.* [26], aerodynamic rotor models of differing fidelity - actuator disc/line and full-rotor - yield largely similar wake characteristics under turbulent inflow. The new SC improves the blade loading in uniform inflow even with low grid resolution, yet the near-wake remains a function of the force smearing - turbulence might change this. Figure 6 shows 10-minute statistics for the blade loading for changing force smearing ($\epsilon/R = \{4, 8, 16\}$). Here results only with SC are presented; for a comparison of blade forces with/without correction refer to [7]. Mean and standard deviation of the forces increase with force smearingand turbulence intensity (TI). The average normal force at the largest ϵ is 3%, the tangential force 5% greater than at the lowest ϵ. The impact on the standard deviation is larger and lies around 10% for both force components. For intermediate smearing, the difference is about halved.

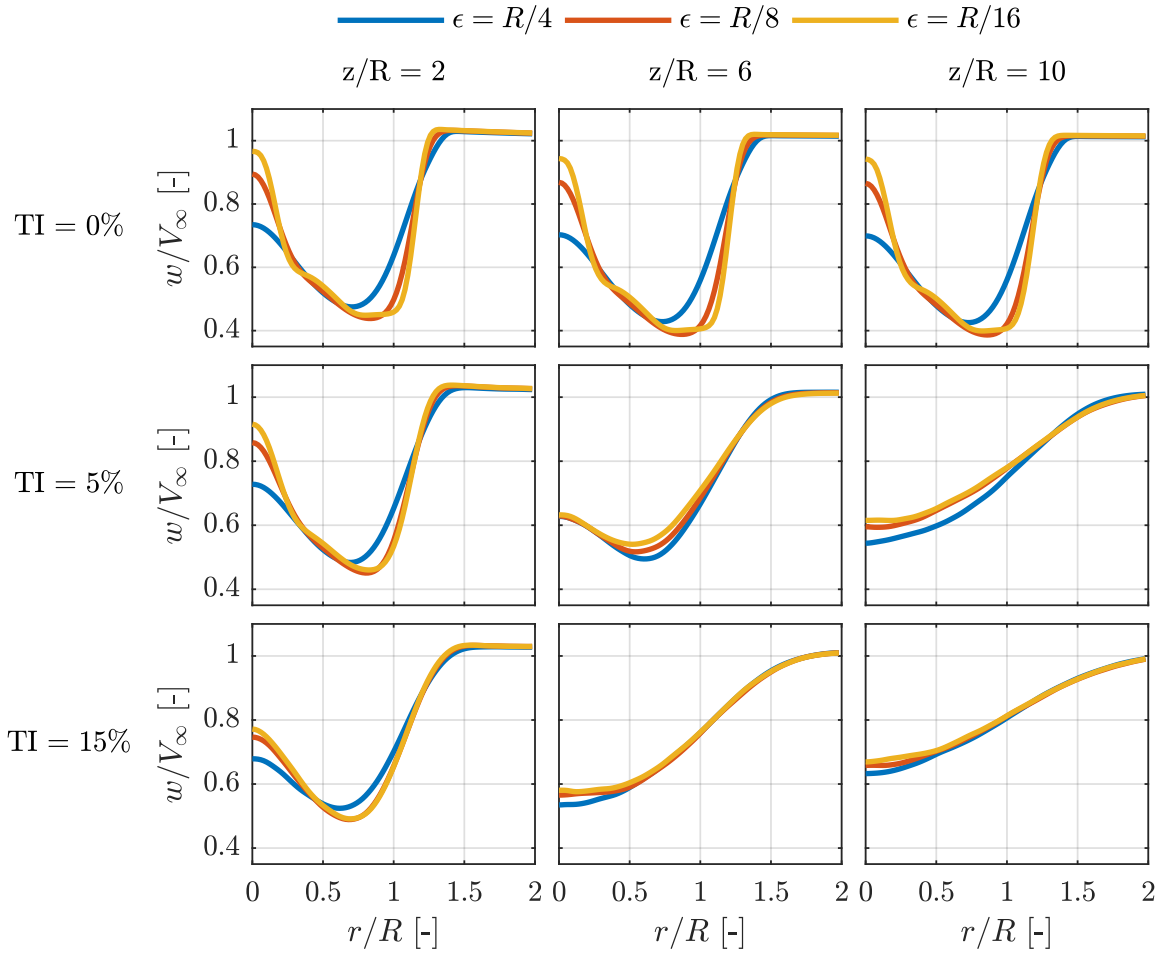

Figure 7. Azimuthally/10-minute averaged wake deficit in three planes downstream of the NREL 5MW and varying turbulence intensity. ($N_v = 36$, $\Delta x = R/32$)

4.2.2. Wakes Figure 7 explores the influence of force smearing in combination with the SC on the downstream evolution of the wake deficit. Without any inflow turbulence, the mean velocity profiles do not evolve after some initial wake expansion. Yet, as shown in figure 5, the shape quickly converges when decreasing the smearing. With inflow turbulence, differences in

the time-averaged profiles largely disappear from $z/R > 6$, rendering them independent of force smearing.

Figure 8 shows a similar behaviour for the standard deviation, only that a more pronounced difference remains between all cases two rotor radii downstream in the regions of the tip and root vortices. This discrepancy directly stems from the force smearing by introducing a viscous core in the shed vorticity, which hinders the break-up of the root and tip vortices. The missing vorticity towards the root for $\epsilon = R/4$, diminishes the rotor added turbulence by about 2% at 5% inflow TI. The lower turbulence intensity six radii from the rotor might explain the deeper deficit observed 4 radii further downstream in figure 7.

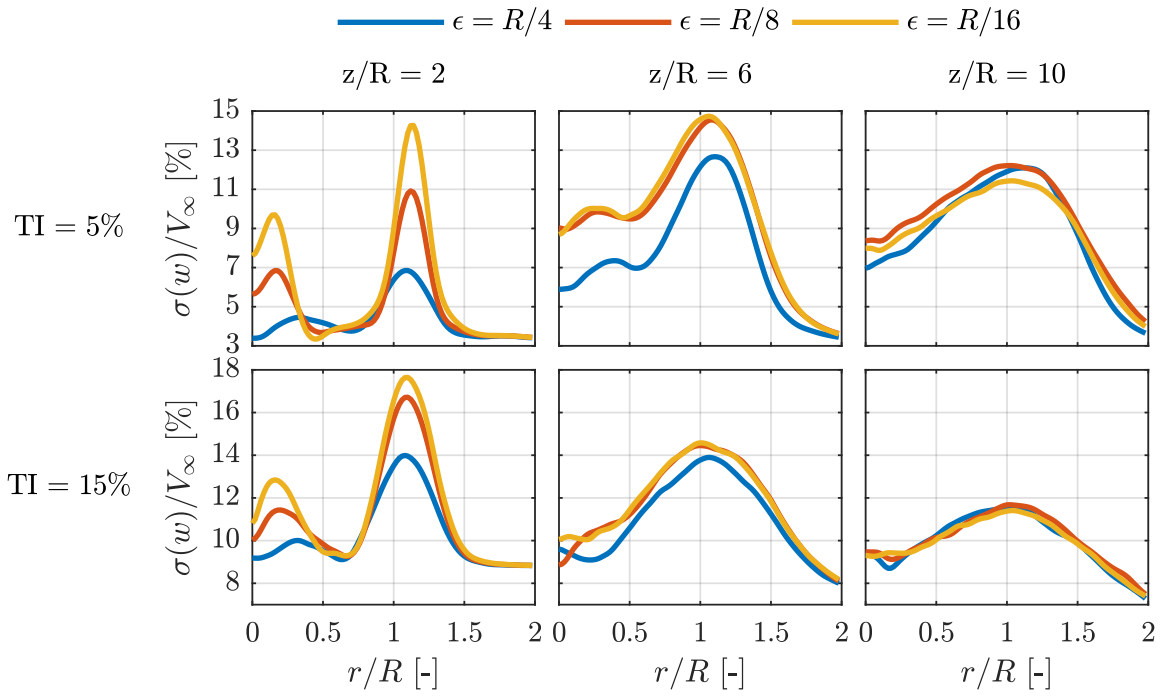

Figure 8. 10-minute standard deviation of the streamwise velocity in three planes downstream of the NREL 5MW and varying turbulence intensity. ($N_v = 36$, $\Delta x = R/32$)

5. Conclusion

The recently developed tuning-free, vortex-based correction that recovers the intended lifting-line behaviour of the actuator line, yields accurate blade forces even at low grid resolution. With only 10 grid cells along the blade, the normal forces are within 3% and the tangential ones within 6% of the reference. It eliminates the force over-prediction towards the root and tip of the standard actuator line and outperforms other more commonly employed tip corrections. The influence of the force smearing on the wake velocities dominates over the choice of correction, yet under turbulent inflow the wake characteristics become nearly independent of force smearing 6 rotor radii downstream of the turbine - this is both for mean and standard deviation of the stream-wise velocity component.

The accurate prediction of blade forces in combination with the correct representation of the rotor wake in turbulent inflow, allows reducing the grid resolution of actuator line simulations, thereby dropping the computational cost of aero-elastic wind farm simulations.

Acknowledgments
We would like to acknowledge DTU Wind Energy's internal project "Virtual Atmosphere" for partially funding this research. Furthermore many thanks to Senior Researcher Dr. Mac Gaunaa for his insights on vortex aerodynamics and Senior Researcher Dr. Niels Troldborg for his input on actuator line simulations/modelling, both from DTU Wind Energy. Thanks also to Ang Li for his help on the near-wake model.

References
[1] Sørensen J and Shen W Z 2002 *Journal of Fluids Engineering* **124** 393–399
[2] Troldborg N, Sørensen J and Mikkelsen R 2009 *Actuator Line Modeling of Wind Turbine Wakes* Ph.D. thesis Technical University of Denmark
[3] Shives M and Crawford C 2013 *Wind Energy* **16** 657–669 ISSN 1099-1824 (*Preprint* `arXiv:1006.4405v1`)
[4] Dag K, Sørensen J, Sørensen N and Shen W 2017 *Combined pseudo-spectral / actuator line model for wind turbine applications* Ph.D. thesis DTU Wind Energy Denmark
[5] Lamb H 1932 *Hydrodynamics* (C.U.P)
[6] Oseen C 1911 *Über Wirbelbewegung in einer reibenden Flüssigkeit* Arkiv för matematik, astronomi och fysik (Almqvist & Wiksells) URL `https://books.google.dk/books?id=wrCJPgAACAAJ`
[7] Meyer Forsting A R, Pirrung G R and Ramos-García N 2019 *Wind Energy Science Discussions* **2019** 1–22 URL `https://www.wind-energ-sci-discuss.net/wes-2018-76/`
[8] Martnez-Tossas L A and Meneveau C 2019 *Journal of Fluid Mechanics* **863** 269292
[9] Pirrung G R, Madsen H A and Schreck S 2017 *Wind Energy Science* **2** 521–532 URL `https://www.wind-energ-sci.net/2/521/2017/`
[10] Pirrung G, Riziotis V, Madsen H, Hansen M and Kim T 2017 *Wind Energy Science* **2** 15–33 URL `https://www.wind-energ-sci.net/2/15/2017/`
[11] Sørensen N 1995 *General purpose flow solver applied to flow over hills* Ph.D. thesis Risø National Laboratory
[12] Michelsen J 1994 Basis3d - a platform for development of multiblock pde solvers Tech. rep. Dept. of Fluid Mechanics, Technical University of Denmark, DTU
[13] Michelsen J 1994 Block structured multigrid solution of 2d and 3d elliptic pdes Tech. rep. Dept. of Fluid Mechanics, Technical University of Denmark, DTU
[14] Meyer Forsting A, Troldborg N, Bechmann A and Réthoré P E 2017 *Modelling Wind Turbine Inflow: The Induction Zone* Ph.D. thesis DTU Wind Energy Denmark
[15] Menter F R 1993 Zonal two equation $k-\omega$ turbulence models for aerodynamic flows 23^{rd} *Fluid Dynamics, Plasmadynamics, and Lasers Conference, Fluid Dynamics and Co-located Conferences* (Orlando,FL)
[16] Strelets M 2001 Detached eddy simulation of massively separated flows 39^{th} *AIAA Aerospace Sciences Meeting and Exhibit* AIAA Paper 2001-0879 (Reno,NV)
[17] Mikkelsen R 2003 *Actuator Disc Methods Applied to Wind Turbines* Ph.D. thesis Technical University of Denmark
[18] Mann J 1998 *Probabilistic Engineering Mechanics* **13** 269–282 ISSN 0266-8920
[19] Ramos-García N, M Mølholm J N S and Walther J H 2017 *Wind Energy, Vol. 20, No. 11, p. 1187-1889.*
[20] Ramos-García N, Shen W Z and Sørensen J N 2014 *Renewable Energy, Vol. 70, p. 78-92. DOI: 10.1016/j.renene.2014.04.001*
[21] Ramos-García N, Shen W Z and Sørensen J N 2014 *Published online in Wind energy. DOI: 10.1002/we.1821.*
[22] Shen W, Sørensen J and Mikkelsen R 2005 *Journal of Solar Energy Engineering* **59** 209–213
[23] Jonkman J, Butterfield S, Musial W and Scott G 2009 Definition of a 5-mw reference wind turbine for offshore system development Tech. rep. NREL
[24] Wimshurst A and Willden R H J 2018 *Wind Energy* 1–14 ISSN 10954244 URL `http://doi.wiley.com/10.1002/we.2177`
[25] Pirrung G R and van der Laan M P 2018 *Wind Energy Science Discussions* **2018** 1–13 URL `https://www.wind-energ-sci-discuss.net/wes-2018-59/`
[26] Troldborg N, Zahle F, Réthoré P E and Sørensen N 2013 *Wind Energy* **18** 10.1002/we.1757